Journal of Sound and Vibration (2000) **234**(4), 681–704
doi:10.1006/jsvi.2000.2891, available online at http://www.idealibrary.com on IDEAL®

MULTICHANNEL FEEDBACK CONTROL FOR THE ISOLATION OF BASE-EXCITED VIBRATION

M. SERRAND AND S. J. ELLIOTT

Institute of Sound and Vibration Research, University of Southampton, Highfield, Southampton, SO17 1BJ, U.K. E-mail: mjs@isvr.soton.ac.uk

(*Received* 16 *June* 1999, *and in final form* 19 *January* 2000)

This paper describes the implementation of an independent two-channel controller based on absolute velocity feedback and its performance in improving the isolation from base vibration of a mounted rigid equipment structure characterized by two-degrees of freedom. A single-channel controller is also investigated. If the base structure were rigid, a collocated control strategy based on feedback of the equipment absolute velocity reduces the vibration transmission by skyhook damping. In this study, the vibrating base is flexible so that no rigid ground is available to react the secondary forces off. The direct velocity feedback (DVFB) control implemented here is shown to be very stable, however, so that high control gains could be applied. Effective damping ratios of up to 600% in the modes of the suspended system could be introduced by the two control channels. The passive isolation performance is thus dramatically improved by the two-channel controller: the heave mode is reduced by up to 40 dB, whereas the amplitude of the pitching mode is attenuated up to 26 dB. The experimental results also show a global improvement in the vibration caused by the resonances of the base plate over the frequency range of control [0–200 Hz]. The control effect decreases with frequency as a consequence of the increasing efficiency of the passive isolation. It is also shown that if the feedback gains are equal for the two control channels, the control effect is the same as adding equal damping terms to the two modal responses of the mounted equipment. Finally, the control is shown to be robust to changes in the plate support dynamics, since adding masses at various positions on the base plate did not destabilize the system.

1. INTRODUCTION

Isolating a piece of equipment from the vibration of a base structure is a very common problem in the field of mechanical engineering. Typically the base vibration is seismic, with an unpredictable waveform and broadband spectrum. Very little can often be done to reduce the base vibration since it is either of high impedance or characterized by complex dynamics and a large number of degrees of freedom. The isolation of any vibration-sensitive equipment from base vibration is therefore usually performed on the transmission paths. Passive isolators are thus widely used to decouple an equipment from a vibrating base structure. However, passive systems for the isolation of equipment from base vibration involve an inherent compromise between good high-frequency isolation, which requires low values of isolator damping, and limited excitation of the rigid-body modes, which requires high values of isolator damping. Soft mountings are generally used since they provide low resonance frequencies of the mounted system and thus reduce the frequency band of vibration amplification. However, if the isolator mounting frequency is too low, there are potentially problems with static stability. Passive isolators thus provide an efficient way of

0022-460X/00/290681 + 24 $35.00/0

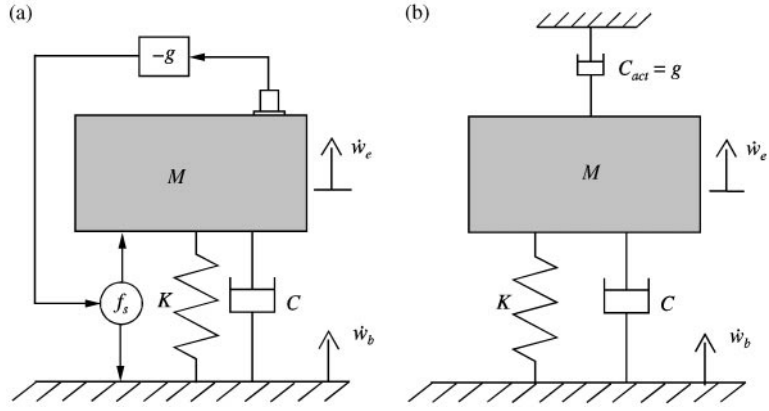

Figure 1. Mechanical effect of absolute velocity feedback control on a single-degree-of-freedom system on rigid base: (a) physical control; (b) mechanical equivalence.

reducing vibration transmission, but they are subject to various trade-offs when excitations with a large frequency range are involved.

Passive isolation performance can be enhanced by coupling active system to the existing mounting design [1]. This can be achieved over a broad frequency band by feedback control strategies, amongst which velocity feedback is one of the most popular since it allows damping to be added in the controlled system. It is thus well known that a single-channel active control system in which a secondary force acts in proportion of the absolute velocity of the mounted equipment, can give good damping in a lumped mass–spring–damper system without compromising the high-frequency isolation [2]. For a secondary force reacting between the mass and the vibrating rigid base, the control has the equivalent effect of a passive damper connecting the mass to an inertial ground as shown in Figure 1. Such a control strategy is thus called skyhook damping.

The transmissibility function with skyhook damping can be written as in equation (1) [3]. The mass motion is then significantly reduced at the resonance frequency by the control without compromising high-frequency performance, as shown in Figure 2, where the modulus of the transmissibility function is plotted for the addition of given amount of extra passive damping or extra active (or inertial) damping:

$$\frac{W_e(\omega)}{W_b(\omega)} = \frac{1 + 2\mathrm{j}\zeta_{pass}\Omega}{1 - \Omega^2 + 2\mathrm{j}(\zeta_{pass} + \zeta_{act})\Omega} \tag{1}$$

where W_e and W_b are the mass and base displacements respectively, $\omega_n = \sqrt{K/M}$, $\Omega = \omega/\omega_n$ is the normalized excitation frequency, C is the passive damping constant, $C_{crit} = 2\sqrt{KM}$ is the critical damping, $\zeta_{pass} = C/C_{crit}$ is the passive damping ratio. $\zeta_{act} = g/C_{crit}$ is the active damping ratio and g is the physical feedback control gain.

The trade-off between damping low-frequency resonances and achieving good high-frequency isolation may thus be overcome by skyhook damping. This was investigated by Schubert [4], who designed a six-channel skyhook damper, which strongly attenuated the vibration of a suspended mass. Skyhook damping implementation was possible using reactive actuators in this case since no base dynamics were taken into account in the frequency range of control, so that an inertial ground was available, as illustrated in Figure 1. Schubert also had a rather complicated controller to give a stable control loop

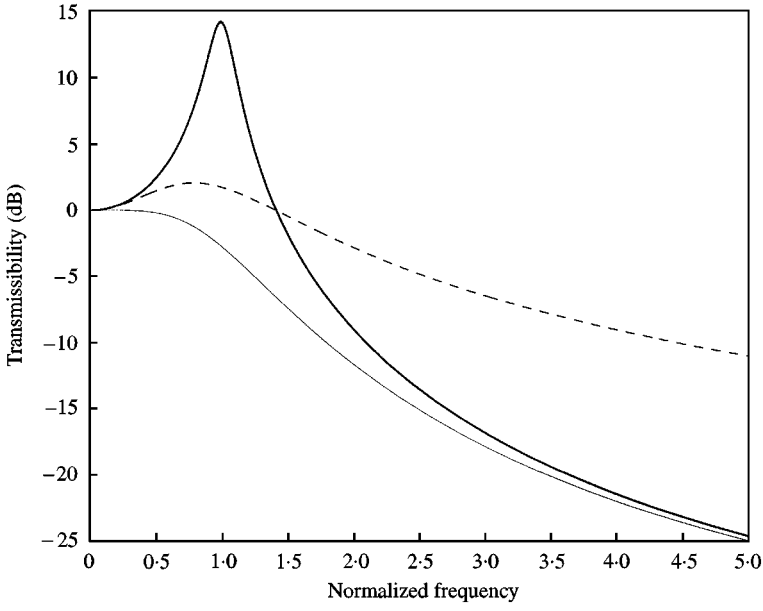

Figure 2. Modulus of the transmissibility for a single-degree-of-freedom system with passive damping, $\zeta_{pass} = 0{\cdot}1$ and no additional damping (——); or with additional passive damping to give, $\zeta_{pass} = 0{\cdot}7$ (- - - -) or with additional skyhook damping, $\zeta_{act} = 0{\cdot}6$ (– –).

whereas, in this study, only constant gain feedback is implemented so that the controller remains as simple as possible. The single- and two-channel controllers studied in this paper generate secondary forces acting in parallel with the passive isolation (Figure 3). Such a combination of passive and active isolations is often referred to in the literature as a soft mount. Beard *et al.* [5] have discussed the advantages of using hard mounts instead of soft mounts, where the secondary actuator is combined in series with the passive isolator. However, the effectiveness of such a mounting design was shown to be dependent upon the high stiffness of the PZT stack used as a secondary actuator. The use of such actuation, characterized by a small deflection capacity, worked well for the small-amplitude motion of the supporting structure considered by those authors. In the study presented here, however, the base vibration can be of the order of millimeters. A soft mount strategy is therefore investigated, in which actuators with a long throw are required, such as electrodynamic shakers, since the active isolation directly connects the equipment to the vibrating base, as shown in Figure 3.

The effect of skyhook damping, as illustrated in Figure 2, has previously been investigated for a infinite impedance base [3, 5] or for a base without significant mobility [4], which is unaffected by the reacting secondary forces. The objective of this study is to investigate the effect of the base structure dynamics on the formulation of direct velocity feedback (DVFB) control. The base structure is said to be "flexible" if it has significant dynamics in the range of control efficiency, i.e. usually if its first modes lie close to the rigid-body resonances of the mounted equipment. In the case of a reactive implementation of the control actuators, the secondary forces are generated by reacting off the base structure. The secondary actuators thus create an addition excitation of the base structure which is transmitted through to the equipment via the mounting system. Because of this mechanical feedback, the classical model of perfect skyhook damping is not valid and the stability of DVFB control, as discussed by Balas [6], has to be reconsidered. In this study,

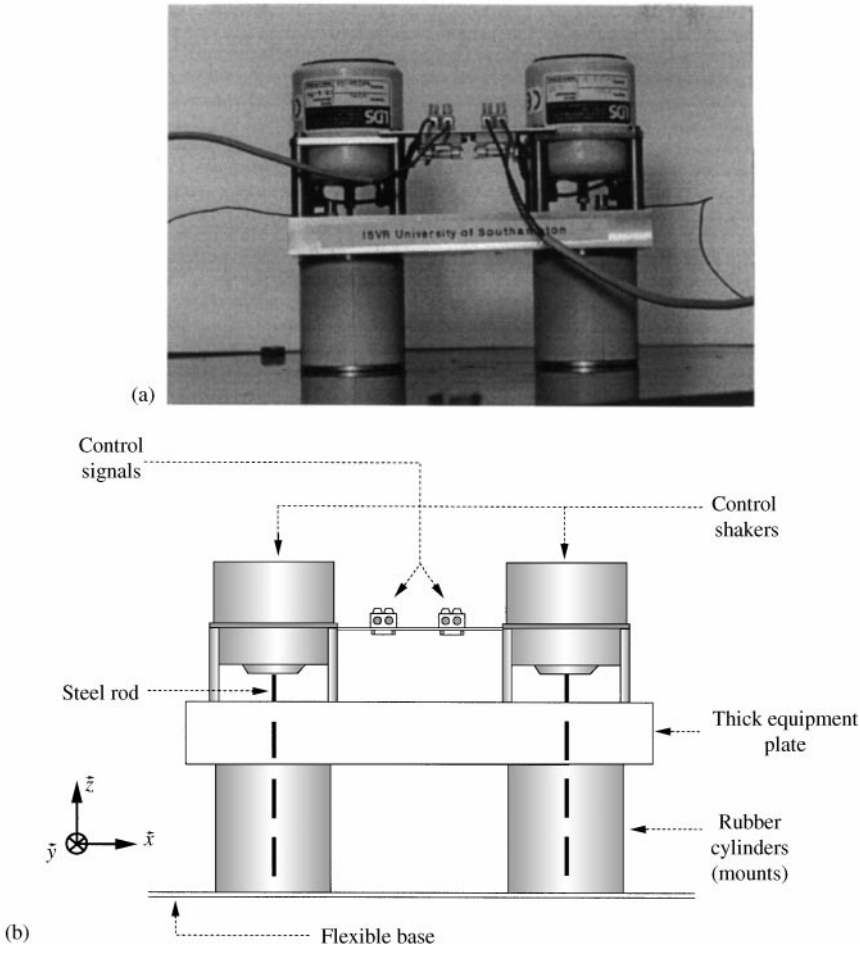

Figure 3. Photograph of the active isolator system (a) and simplified schematic (b).

close attention was therefore paid to the assessment of the system stability before any control implementation.

2. ISOLATION SYSTEM DYNAMICS

2.1. EXPERIMENTAL ISOLATION SYSTEM

The experimental isolation system consists of a rigid piece of equipment mounted on a vibrating plate through two passive/active mounts. The equipment to be isolated and the passive and the active isolators are together referred to as the active isolator system. The active isolator system consists of the two passive/active mounts symmetrically set underneath the equipment structure as shown in Figure 3. The equipment structure is composed of a thick aluminium plate (200 mm × 100 mm × 18 mm) and the two control shakers which are rigidly connected to it. This assembly behaves as a rigid body in the frequency range of interest [0–200 Hz]. The passive part of the mounts consists of a moulded ring of rubber mounted between two aluminium discs. The top disc is rigidly

connected to the equipment structure while the bottom disc is bonded to the vibrating base plate. A thin steel rod inside each ring of rubber transmits the axial force generated by the control shaker to the bottom disc of the mount. The control forces therefore act in parallel with the passive isolation. The control shakers are electromechanical devices (Ling type V101). Each actuator can deliver a maximum force of 8·9 N peak and can provide a maximum peak-to-peak displacement of 2·5 mm. The force generated is proportional to the product of the instantaneous current in the coil and the magnetic flux density. In the frequency range of application, the input voltage to the actuator is proportional to the current in the moving coil since the inductance effect is negligible compared to the shaker electrical resistance. Moreover, in this frequency range, for each shaker, the motional impedance is negligible compared to the blocked impedance so that the control force is proportional to the current and thus to the input voltage. The voltage can then be used as the control quantity and only a standard power amplifier is required in the control loop. More details on the active isolator system may be found in references [7, 8].

A steel rectangular plate (500 mm × 700 mm × 2 mm) clamped along the two long opposite edges and free at the two others was used as the experimental base structure. The plate had sufficient static rigidity to support the equipment and could be driven by a primary shaker to provide a sufficient velocity on the receiver to overcome any signal-to-noise problems, even though the passive isolation can provide strong vibration attenuation above the mounted system resonances.

2.2. ISOLATION SYSTEM DYNAMICS

2.2.1. *Active isolator system dynamics*

The whole system is excited by an out-of-plane force generated by a primary shaker acting on the base plate. The primary excitation will excite flexural modes of the plate which, in general, will induce vertical translation and rotation at the base of the mounts. This will thus mainly excite the heave mode and rocking mode of the mounted equipment (Figure 4) both of which can be controlled by the two actuators.

Other rigid-body modes of the mass such as the transverse one along $\vec{x}$ may be excited by the rotation of the rubber mount discs, but in practice their amplitude is observed to be small since the rotational excitation on the plate is not important compared to the axial plate motion at low frequencies [9]. Finally, since no resonance occurs in the mounts in the frequency range [0–200 Hz], the active isolator system can be quite accurately modelled at low frequencies as a two-degrees-of-freedom system with decoupled passive and active contribution as shown in Figure 5 [8]. In this figure K and C are the axial stiffness and damping constants resulting from one ring of rubber, the steel rod and the shaker suspension, and f_{s1} and f_{s2} are the secondary forces generated by the control shakers.

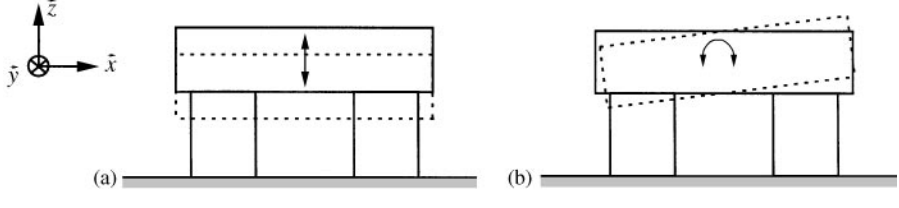

Figure 4. Excited rigid-body modes of the isolator system considering a rigid receiver. Heave mode (a) and pitching mode (b).

TABLE 1

Summary of the passive properties of the experimental mounts and the receiving system

Parameter	Value
Total mass of the thick receiving plate and shakers	$M = 2{\cdot}9$ kg
Moment of inertia of the total mounted system	$I_r = 1{\cdot}4 \times 10^{-2}$ kg m^2
Total stiffness of each mount	$K = 24\,000$ N/m
Total viscous damping for each mount	$C = 18$ N s/m
Effective heave mode damping ratio	$\zeta_h = 4{\cdot}8\%$
Effective pitching mode damping ratio	$\zeta_p = 5{\cdot}1\%$
Distance between mounts	$2l = 134$ mm

Note: The damping constant C was calculated from the measured heave mode damping ratio ζ_h. The pitching mode damping ratio, ζ_p, was also estimated experimentally under normal conditions of temperature and pressure

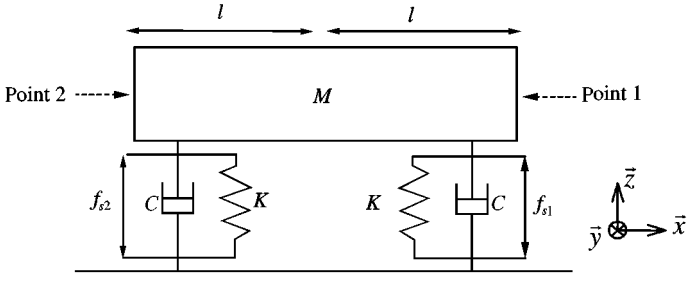

Figure 5. Isolator system mechanical model.

Table 1 lists the main characteristics of the elements of the experimental active isolator system. The heave resonance frequency f_h and the pitch resonance frequency f_p can be estimated using equations (2) and (3), in which I_r is the moment of inertia of the total suspended equipment around the $\bar{y}$-axis, which give 20·5 and 19·8 Hz respectively,

$$f_h = \frac{1}{2\pi}\sqrt{\frac{2K}{M}} \quad \text{and} \quad f_p = \frac{1}{2\pi}\sqrt{\frac{2Kl^2}{I_r}}. \tag{2, 3}$$

The response of the rigid-body modes of the experimental equipment were measured by placing the active isolator system on a rigid base and driving the two control shakers in phase to excite the heave mode and out of phase to excite the pitching mode. The measured natural frequency of the heave resonance was found to be slightly lower than that of the pitch one, 19·1 and 20·7 Hz respectively, but the two frequencies are so close to those predicted theoretically that the simple analytical model shown in Figure 5 can still be used to understand the results of the subsequent tests.

2.2.2. *Base plate dynamics*

The plate was modelled using a modal approach, accounting only for bending motion and assuming an isotropic thin flat plate with beam mode shapes of equivalent boundary conditions as defined by Warburton [10]. The base plate dynamics were also experimentally investigated by measuring, at different locations, the acceleration responses of the

plate alone under primary excitation. The measured and calculated natural frequencies are given in Table 2. The measured natural frequencies are in reasonable agreement with the predicted ones, except for the lowest modes, since the arrangement used to fix the base plate does not completely clamp the two longest edges at low frequencies. All the natural frequencies of the plate are above those of the experimental isolator system, but are sufficiently close to them that the base plate will have a significant dynamic effect on the system response and cannot be regarded as being rigid over the frequency range of interest.

2.2.3. *Coupled system dynamics*

The active isolator system was then mounted on the vibrating plate, positioned so that both the heave and pitch motions of the equipment were excited as shown in Figure 6.

Figures 7 and 8 show the velocity response at points 1 and 2 (see Figure 5) on the equipment per unit primary excitation force f_0, i.e., the passive system response at the two control locations. This measure of the system response was preferred to transmissibility since in this experiment the base plate is flexible, which means not only that different measurement locations on the vibrating plate produce different transmissibilities but also that the reacting control forces affect the plate vibration thus rendering any interpretation of the controller performance rather difficult. The first two main peaks noticeable in Figures 7 and 8 are related to the rigid-body modes of the mounted equipment. The heave mode is shifted down to 14·6 Hz whereas the pitch resonance occurs at 19·8 Hz, since the active isolator system is now coupled to a flexible structure which lowers the effective stiffness of the system. The overall response drops with increasing frequency as the passive isolation starts to become more efficient. As expected, the base plate dynamics appear to have a large effect on the equipment velocity response, which is significantly amplified at the plate resonances. Also shown in Figures 7 and 8 are the predicted values of the equipment

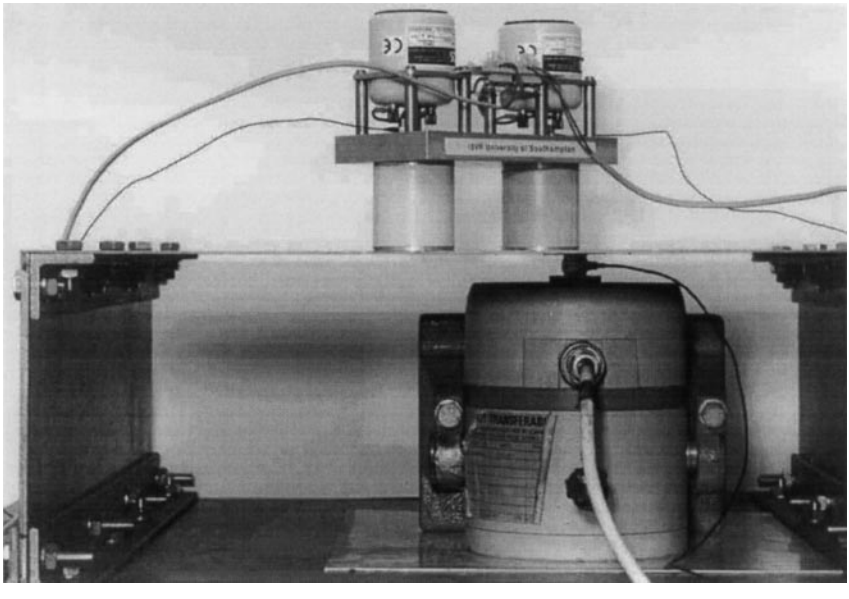

Figure 6. Photograph of the complete isolation system: active isolator system set on top of the flexible base plate excited by a primary shaker.

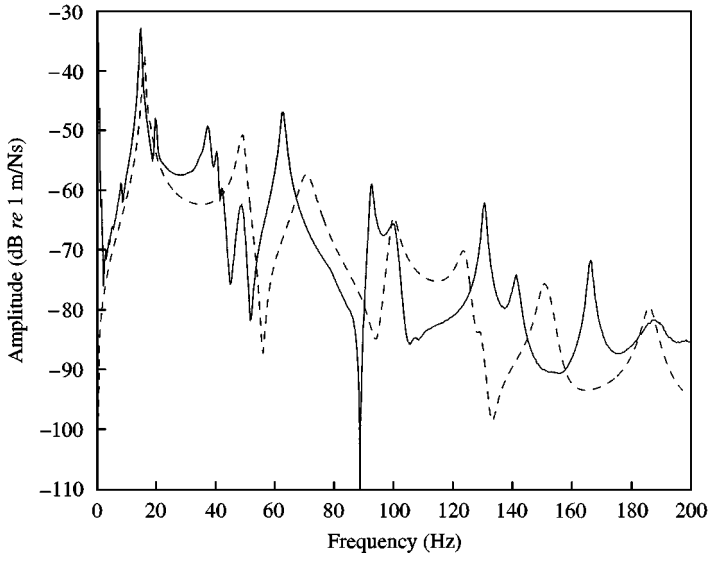

Figure 7. Velocity of the equipment at point 1 per unit primary excitation force without control: measurement (——) and simulation (– – –).

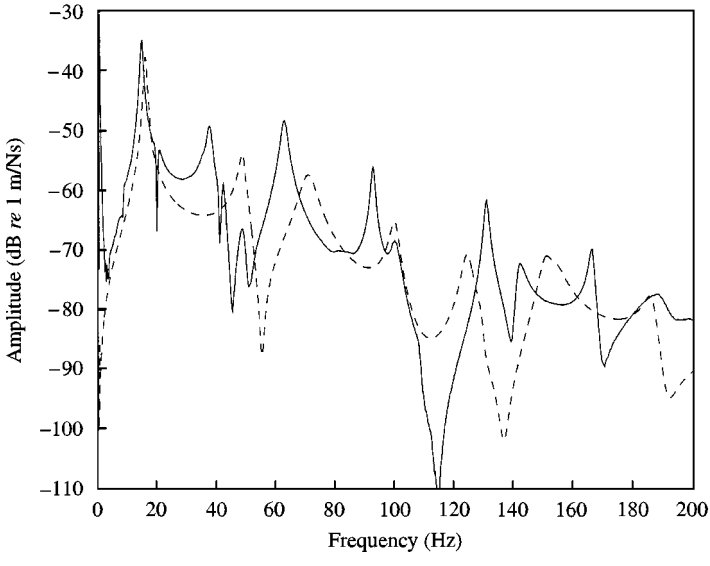

Figure 8. Velocity of the equipment at point 2 per unit primary excitation force without control: measurement (——) and simulation (– – –).

velocity per unit primary force f_0 calculated from a fully coupled simulation of the combined dynamics of the base plate and active isolator system. The measured and predicted responses are in reasonable agreement, considering the discrepancies shown in Table 2, particularly for the low-frequency response. The good matching between experiments and simulations suggests that the dynamics can be understood using the simple models outlined above.

TABLE 2

First 9 modes of the base supporting plate

Mode	Experimental frequency (Hz)	Calculated frequency (Hz)	Mode shape
(2, 0)	32·5	44·8	
(2, 1)	41·3	49·0	
(2, 2)	58·8	65·4	
(2, 3)	91·3	98·8	
(3, 0)	99·8	123·3	
(3, 1)	105·0	129·2	
(3, 2)	128·0	149·8	
(2, 4)	139·0	151·8	
(3, 3)	166·2	186·0	

(m, n): m is the number of nodal lines relative to the CC boundary conditions and n is the number of nodal lines relative to the FF boundary conditions.

3. CONTROL PRINCIPLE AND EXPERIMENTAL ARRANGEMENT

The objective of the study was to implement two independent channels of velocity feedback to give skyhook control using two reactive actuators. The output of the control sensor associated with each control location is therefore directly fed to the corresponding secondary actuator, so that two single-input–single-output (SISO) control loops are implemented as sketched in Figure 9. Decentralized control algorithms have the advantage of being very simple to implement, with the complexity rising linearly with the number of channels instead of with the square of the number of channels in a fully coupled controller, and have also been implemented for the feedforward control of periodic disturbances [11, 12].

The control sensor at each control point is an accelerometer, B&K type 4375. The acceleration signal is integrated through a charge amplifier, B&K type 2635. The resulting voltage signal, y, which is ideally proportional to the equipment velocity, is amplified by a constant control gain g_c using a power amplifier and fed back to the control shaker. Each secondary actuator thus applies a secondary force which is only the result of the velocity at the corresponding control point. However, the control input u_1 does not only induce a velocity at point 1 but also a response at point 2, and similarly for u_2, as expressed in the equation

$$\mathbf{y} = \begin{bmatrix} y_1 \\ y_2 \end{bmatrix} = \begin{bmatrix} G_{11} & G_{12} \\ G_{21} & G_{22} \end{bmatrix} \cdot \begin{bmatrix} u_1 \\ u_2 \end{bmatrix} = \mathbf{G} \cdot \mathbf{u}, \tag{4}$$

where $\mathbf{y}$ is the output voltage vector, proportional to the outputs of the accelerometers on the equipment after integration by the charge amplifiers, G_{ij} is the plant response at point i for an excitation at point j, $\mathbf{G}$ is the plant response matrix including the secondary actuators and $\mathbf{u}$ is the secondary actuator input voltage vector.

The two control locations are mechanically coupled, which is not explicitly taken into account by the controller. The mechanical coupling was measured by exciting the whole system with one of the control shakers and measuring the resulting velocity at the control points on the equipment. Figure 10 shows the measured velocity at point 1 per unit shaker input voltage when the equipment is excited by the control shaker 1 (u_1) and when it is

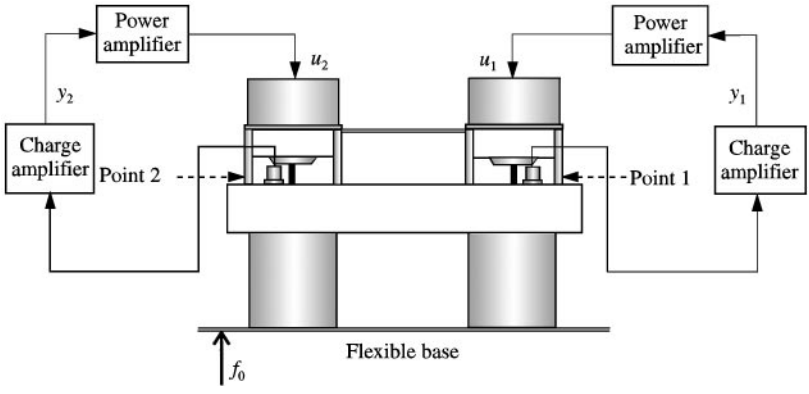

Figure 9. Schematic of the two independent channel control implementation.

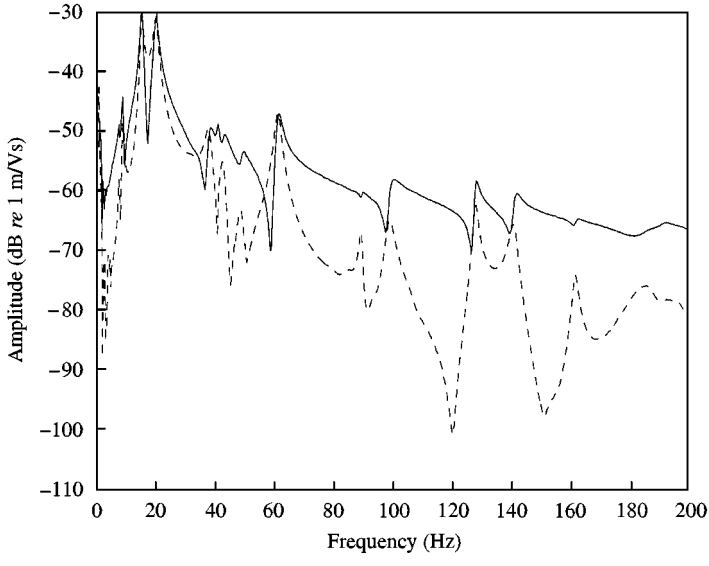

Figure 10. Measured velocity of the equipment at point 1 for excitation from the control shaker at point 1 (——) and from the control shaker at point 2 (– – –).

excited by the control shaker 2 (u_2), and Figure 11 shows the same quantities for point 2. The sensitivity of the sensors has been used to obtain the velocity responses in Figures 10 and 11 in mechanical unit. These graphs represent, to the sensor sensitivity factor, the frequency responses of the four elements of the plant response matrix **G** in equation (4).

From these measurements, it appears that the coupling between the two control points is significant at the natural frequencies of the rigid-body modes, since the rigid-body modes generate the same amplitude of vibration at the two ends of the mounted system. The coupling is also significant at the plate resonances, but decreases with increasing frequency as the passive isolators become more effective. These measured plant responses were used in the assessment of the stability of the combined control system.

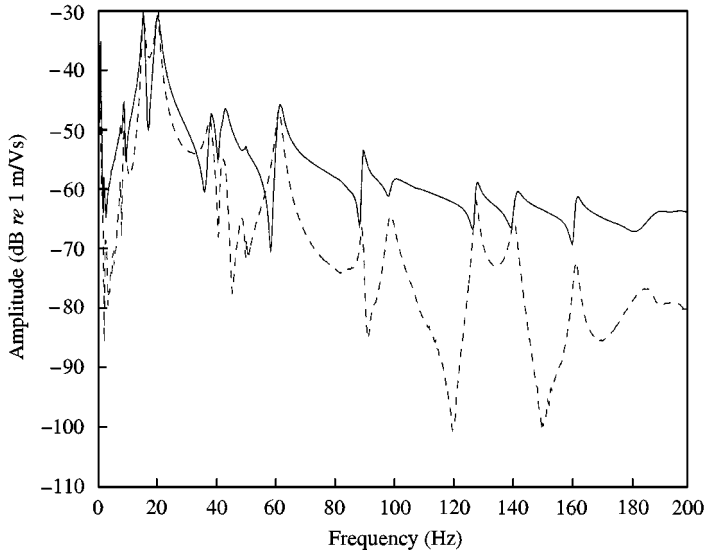

Figure 11. Measured velocity of the equipment at point 2 (———) and from the control shaker at point 2 (– – –) and from the control shaker at point 1 (– – –).

4. FEEDBACK CONTROL PRINCIPLES

Considering the equivalent electrical block diagram of a multichannel feedback control system (Figure 12), the response of the controlled system can be derived and expressed in the Laplace form as

$$\mathbf{y}(s) = [\mathbf{I} + \mathbf{G}(s)\mathbf{H}(s)]^{-1}\mathbf{d}(s) \tag{5}$$

where $\mathbf{I}$ is the identity matrix, $\mathbf{y}$ is the sensor output signal vector of the system under control, $\mathbf{d}$ is the vector of disturbances which is the sensor output signal vector with no control, $\mathbf{G}(s)$ is the transfer function matrix of the plant defined by equation (4) and $\mathbf{H}(s)$ is the matrix of feedback gains, which in this case is diagonal.

Instability can be associated with the poles of the system, i.e., the values of s which satisfy the characteristic equation [13, 14]

$$\det[\mathbf{I} + \mathbf{G}(s)\mathbf{H}(s)] = 0. \tag{6}$$

The general Nyquist criterion states that provided the plant and controller are themselves stable, the closed-loop system will be stable if the complex locus of the expression

$$\det[\mathbf{I} + \mathbf{G}(\mathrm{j}\omega)\mathbf{H}(\mathrm{j}\omega)] = (1 + \lambda_1(\mathrm{j}\omega))\cdot(1 + \lambda_2(\mathrm{j}\omega)) \tag{7}$$

does not encircle the origin as ω goes from $-\infty$ to $+\infty$, where $\lambda_1(\mathrm{j}\omega)$ and $\lambda_2(\mathrm{j}\omega)$ are the two eigenvalues of the (2×2) matrix $\mathbf{G}(\mathrm{j}\omega)\mathbf{H}(\mathrm{j}\omega)$. This implies that none of the frequency-dependent eigenvalues of $\mathbf{G}(\mathrm{j}\omega)\mathbf{H}(\mathrm{j}\omega)$ must encircle the point $(-1, \mathrm{j}0)$ when the frequency is varied over this range [14]. When an identical control gain g_c is used in both

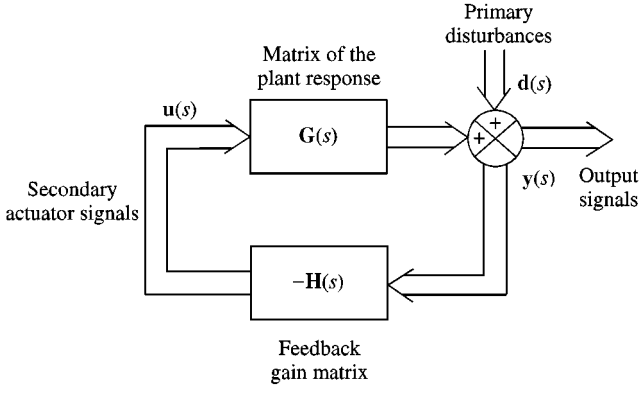

Figure 12. Equivalent electrical block diagram of a multichannel feedback control system.

control channels, the feedback gain matrix is simply

$$\mathbf{H}(\mathrm{j}\omega) = \mathbf{H} = \begin{bmatrix} g_c & 0 \\ 0 & g_c \end{bmatrix}. \tag{8}$$

The stability assessment thus simplifies to the study of the Nyquist plot of the eigenvalues of the plant response matrix $\mathbf{G}(\mathrm{j}\omega)$.

For the special case of a single-channel feedback control [13], the transfer function estimating the attenuation provided by the control is simply

$$\frac{y_i(s)}{d_i(s)} = \frac{1}{1 + G_{ii}(s)H_{ii}(s)}. \tag{9}$$

If the feedback controller, $H(s)$, is a simple amplification by a constant gain, the single-channel control stability can be assessed by examining the Nyquist plot of the single plant response $G_{ii}(\mathrm{j}\omega)$.

5. SINGLE-CHANNEL CONTROL

Prior to implementing the two-channel controller, a single-channel DVFB control was implemented at one end of the the equipment. This was done to evaluate the effect of the control at the other end and to assess the extent to which a system characterized by two-degrees of freedom could be isolated from a vibrating structure with only a single secondary force. The results presented in this section refers to a single-channel control a point 1 only (see Figure 9).

5.1. STABILITY ASSESSMENT

Figure 13 shows the Nyquist plot of the plant response $G_{11}(\mathrm{j}\omega) = y_1(\mathrm{j}\omega)/u_1(\mathrm{j}\omega)$ for this case.

The system exhibits very good stability properties since almost the whole polar diagram lies in the positive real half-plane. It is characterized by two main loops caused by the heave

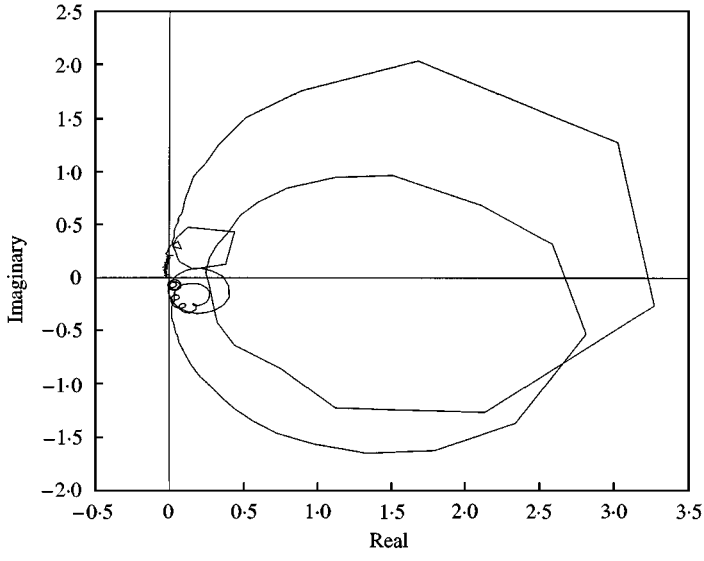

Figure 13. Nyquist plot of the plant response G_{11} for a local control of the equipment at point 1.

and pitching modes of the mounted equipment. Finally, the base plate resonances lying in the frequency range [0–200 Hz] are represented by several small circular loops whose radius decreases as the passive isolation becomes more efficient with increasing frequency. They are mainly located in the positive real part half-plane but not fully. Therefore, the measured plant response does not have a strictly positive real part at all frequencies, and thus differs from the input mobility which would be measured if the actuator only acted at the control point, without having to react off the flexible base structure. These mechanical effects are not large, since the absolute value of the phase is never significantly larger than $\pi/2$, and are always associated with small amplitudes as a result of the passive isolation. The additional phase shift due to the flexible base thus does not appear to cause any noticeable stability problem or amplification of the equipment motion. A further discussion of the stability of a single-channel active isolation system with either a reactive or inertial actuator is provided by Elliott *et al.* [15].

At very low frequencies however (<2 Hz), the control is affected by the frequency response of the integrator in the charge amplifier, whose associated lowpass filter is responsible for an additional phase shift which tends to $\pi/2$ at very low frequencies. This is not expected to cause instability but will give rise to very low-frequency amplification. This has to be added, however, to the low-frequency phase shift of the power amplifier. These low-frequency phase shifts are the cause of the small response noticed on the upper left side of the origin in Figure 13, and can give rise to instability if the control gain is very large.

5.2. CONTROL RESULTS

Figure 14 shows the velocity at point 1 on the equipment per unit primary force f_0 measured for three control gains, as listed in Table 3.

It shows that the passive isolation is significantly improved by the controller at point 1. The vibration of the mass at the location of the control sensor is gradually reduced over the whole frequency range displayed as the gain is increased. The vibration level is reduced by

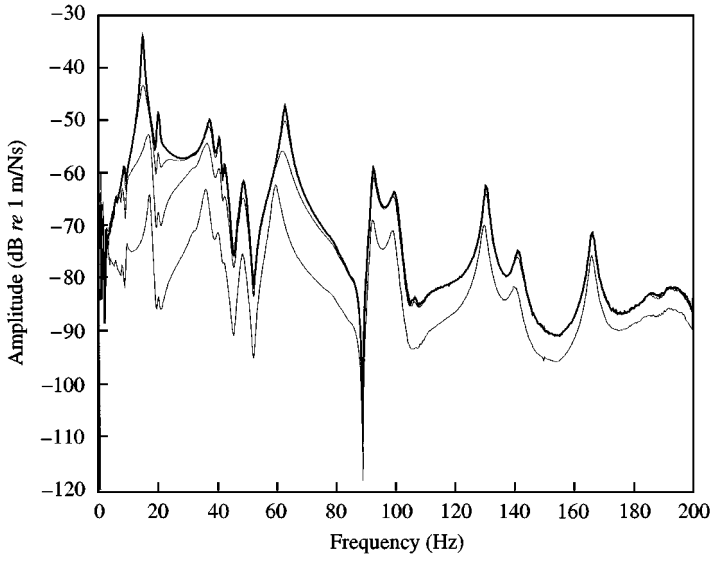

Figure 14. Measured velocity of the equipment at point 1 per unit primary force for a single channel control at point 1. Measurements are shown for the passive system (control off) (———) and three values of physical control

TABLE 3

Values of feedback control gains and the corresponding active damping ratios due to one control channel

Physical control gain g (N/m s)	Equivalent active damping ratio of the heave mode ζ_{hact}	Equivalent active damping ratio of the pitching mode ζ_{pact}
55	0·07	0·08
278	0·37	0·40
720	0·96	1·02
2285	3·05	3·29

up to 40 dB at the heave mode passive resonance frequency. As expected, the effect of the controller gradually decreases with increasing frequency since the control force is proportional to the control velocity which is strongly attenuated by the passive isolation at high frequencies. Amplification is, however, noticed at very low frequencies, although this does not corrupt the overall improvement of the passive isolation. For the highest value of feedback gain used, however, the system under control becomes very reactive to external transient excitations in the laboratory because of the low-frequency instability discussed above in the plant response analysis.

Even if the control is not strictly equivalent to skyhook damping, the first component of the secondary force acting directly on the equipment does have the mechanical effect of a skyhook damper and an equivalent active damping ratio due to one control channel can be calculated to compare with the passive damping ratios of the heave and pitching modes of the mounted system, ζ_h and ζ_p. The values of the physical control gain g (gain relating the secondary force to the control velocity in units of Ns/m) and the equivalent active damping ratios associated with the heave mode, ζ_{hact}, are listed in Table 3 when calculated

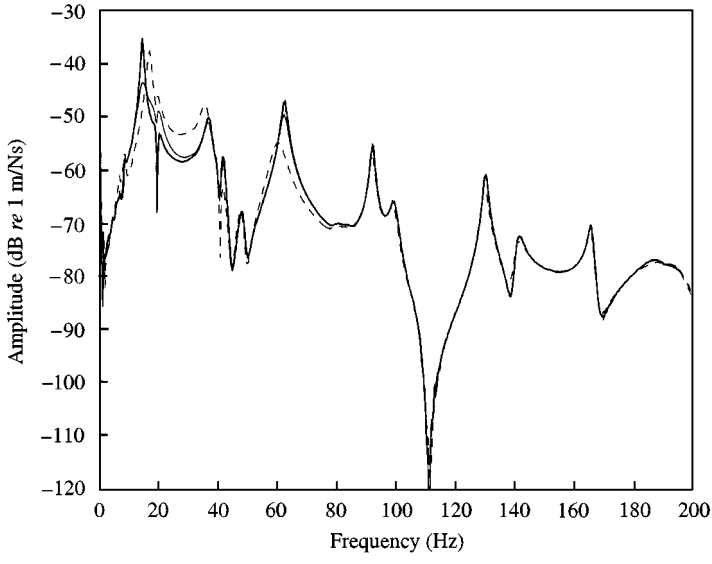

Figure 15. Measured velocity of the equipment at point 2 per unit primary force for a single channel control at point 1. Measurement are shown for the passive system (control off) (———) for physical control gain of $g = 55$ (——) and $g = 720$ (– – –).

using

$$\zeta_{hact} = \frac{g}{2C}\zeta_h, \tag{10}$$

where C is the passive damping constant for a rubber mount and the physical control gain, g, is calculated from the electrical control gain, g_c, using the equation

$$g = g_c S_{sh} S_{ca}, \tag{11}$$

where S_{sh} is the sensitivity of one control shaker (equal to $0{\cdot}91\,\mathrm{N\,v^{-1}}$) and S_{ca} is a multiplicative factor applied by the charge amplifier when it is used as an integrator (equal to 100). As an example, the maximum physical gain g of 2285 Ns/m corresponds to a control gain g_c from the power amplifier equal to 25. This calculation is meaningful since the responses of the actuators and sensors were reasonably independent of the frequency. The equivalent active damping ratio in the pitching mode, ζ_{pact}, is also calculated using equation (10), but using the passive damping ratio in the pitching mode, ζ_p.

Figure 15 shows the effect of the feedback loop acting at end 1 on the equipment velocity at the other end for two of the values of feedback gain listed in Table 3. The controller does not greatly affect the motion of the mass at point 2 in comparison with the improvements obtained at the control point. It tends, however, to amplify the vibration level in some frequency bands for the use of high feedback gains, which give rise, for instance, to a 6 dB increase between about 15 and 35 Hz. No real effect of the control is observed above 80 Hz as expected from the weak mechanical coupling between the control points shown in Figures 10 and 11. Similar stability properties and performance at the two ends of the equipment are observed when a single-channel control system is implemented at point 2 [7].

6. IMPLEMENTATION OF A TWO-CHANNEL CONTROLLER

6.1. STABILITY ASSESSMENT

The stability of the two-channel control system, as shown in Figure 9, was assessed using the procedure outlined in section 4. Figures 16 and 17 show the two Nyquist plots for the frequency-dependent eigenvalues λ_1 and λ_2 of the plant response matrix **G** defined in section 3. One should note that, for this special arrangement, the two eigenvalues are

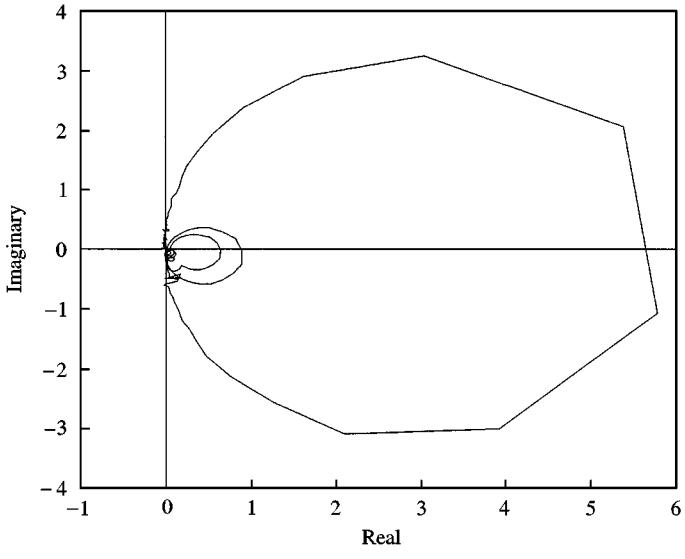

Figure 16. Nyquist representation of the eigenvalue λ_1 associated with the heave motion of the suspended equipment.

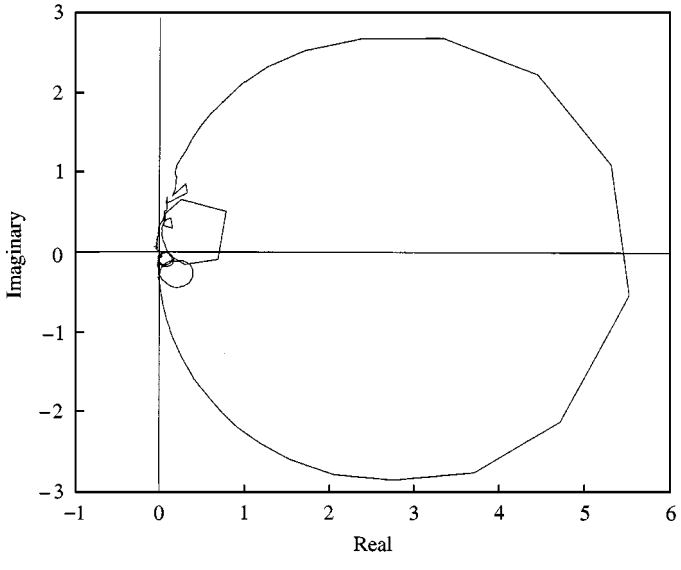

Figure 17. Nyquist representation of the eigenvalue λ_2 associated with the pitching motion of the suspended equipment.

proportional to the amplitudes of the heave and pitch modes of the equipment motion and thus each of them only has one main loop. The two plots illustrate the stable properties of the controlled system. Most of the loci lie in the stable right half-plane and strong vibration reductions were therefore expected. The contour slightly crosses the imaginary axis at frequencies above the mounted system resonances. This is due to the base plate dynamics, as discussed in the single-channel control implementation in section 5, but no instability or significant vibration amplification could arise by the application of a simple control gain. The main threat to the control stability again comes at low frequencies from the phase shifts in the electronics of the control loop as for the single channel case above.

6.2. RESULTS

Figures 18 and 19 show the velocities measured at the two control points on the equipment when both control loops are simultaneously closed for three values of feedback gain g, as listed in Table 3 with the corresponding effective active damping ratios. The same gains were used for both control channels. As expected from the stability assessment, very large reductions of the receiver vibration are achieved at the two sensor locations without stability problems. This shows that the isolation of the equipment from base motion has been considerably improved over the full frequency range of measurements, except at very low frequency, below 2 Hz. Above 2 Hz, the larger the feedback gain, the larger the reduction of the vibration level. Particularly large reductions of the equipment vibration are observed at the resonances of the two rigid body modes, thus fulfilling the original objective of this control strategy. The amplitude of the heave resonance drops by up to 40 dB for the highest feedback gain, whereas the amplitude of the pitching mode at resonance is attenuated by up to 26 dB since it was originally less excited. The heave resonance is no longer noticeable after control for the highest values of gain, whereas it was in the previous single-channel control. The overall mass motion is also strongly attenuated at the plate

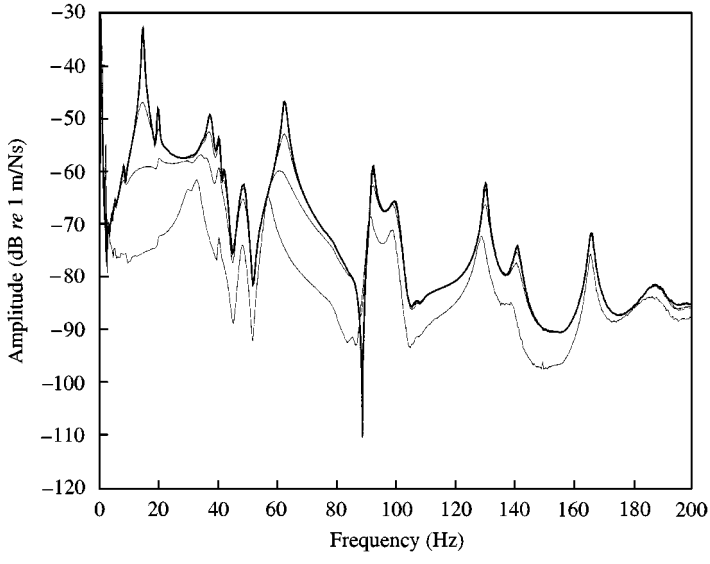

Figure 18. Measured velocity of the equipment at point 1 per unit primary force for two channel control. Measurements are shown for the passive system (control off) (———) and three values of physical control gain (——): 55, 278 and 2285, which give progressively lower values of response.

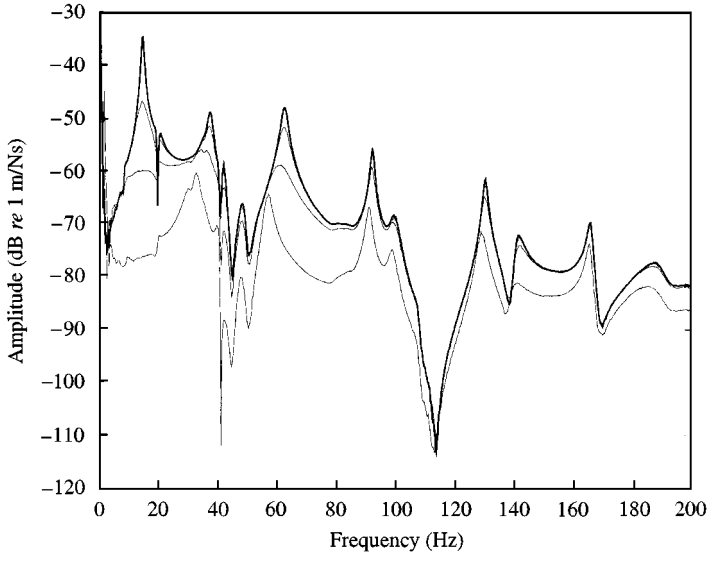

Figure 19. Measured velocity of the equipment at point 2 per unit primary force for two channel control. Measurements are shown for the passive system (control off) (———) and three values of physical control gain (——): 55, 278 and 2285, which give progressively lower values of response.

resonances (by 16 dB for the third plate resonance at 62 Hz) which are slightly shifted down in frequency under the effect of the additional active damping. As the passive isolation performance increases, the control effect decreases and only 3–4 dB reductions are obtained at 200 Hz and no real improvements are observed above this frequency.

Significant amplifications of the very low-frequency response of the mass can be noticed in Figures 18 and 19 at high feedback gains. No instability was encountered for steady running conditions unless the gain g was increased beyond the range reported in Table 3. Little low-frequency enhancement was encountered for lower control gains, which can still give significant attenuation of the the mounted system resonances. For example, a gain g of 278 introduces skyhook dampers with an equivalent damping constant 15 times bigger than the passive damping constant C (see Table 3) and provides a 27 dB reduction of the amplitude of the heave mode resonance and almost a 10 dB attenuation of the amplitude of the pitching mode resonance. The gain margin for the control loop with this feedback gain is then greater than 20 dB.

The two-channel DVFB controller is thus a very simple and robust control strategy which can give significant improvements in the isolation performance offered by the passive system. The flexibility of the support did not significantly degrade the isolation efficiency of the feedback controller in this case, as it may have been expected. To reinforce this experimental result, further experiments were carried out on the system by adding a mass of 4·1 kg, which is comparable to the mass of the base plate (5 kg), positioned at five different locations. Although the added mass lowers the first base plate resonance frequency close to the isolator system resonances, the control system appeared, from the plant response measurements, to remain as stable as in the previous analysis, up to feedback gains of the same order as for the control system detailed above. Similar reductions could thus be expected. The control is still limited at low frequencies by the electronics in the control loop but not by the system dynamics. This demonstrates that the good results shown in Figures 18 and 19 are not only specific to the mechanical system considered. A reactive implementation of DVFB control appears to be robust to change in the base plate dynamics.

7. CONCLUSIONS

The implementation of a two independent channel DVFB control led to very significant improvements of the passive isolation capacity of the experimental arrangement detailed here, since the dynamics of the equipment to be isolated was almost fully defined by two axial degrees of freedom. The main trade-off in the use of passive mounts for vibration isolation is overcome since the resonance of the rigid-body modes of the equipment are almost completely cancelled without degrading the high-frequency performance of the passive mounts. The control also improves the isolation above the mounted system resonances up to frequencies where the passive isolation becomes very efficient whereas instability could have been expected from the base flexibility. One of the main findings of this study is that no instability or vibration amplification was encountered from potential re-excitation of the flexible base by the secondary actuators in the frequency range of analysis. The control is therefore very close to perfect skyhook damping. Moreover, changes in the dynamics of the base plate did not destabilize the control system, illustrating its robustness. This suggests that multichannel DVFB control using reactive secondary forces can be considered for application on other flexible base structures.

These results were achieved for a very simple decentralized control implementation which did not explicitly account for any coupling between the control channels. If the base had been rigid, each channel would synthesise a passive skyhook damper at the control points because the actuator and sensor for each control channel are collocated and the stability of each control loop is in principle unaffected by the presence of the others. In the practical problem considered, however, mechanical cross-talk between the channels is induced by the base plate dynamics and such a statement is no longer valid. Subsequent analysis of the decentralized control system implemented has revealed that it is exactly equivalent to a modal control system under the condition of identical feedback gains in the two channels. This equivalence is presented in detail in Appendix and gives an initial explanation of the performance of the independent channel controller since the active isolator system was set on the base plate such that no significant coupling between the heave and pitch mode could arise from the base flexibility. The two-channel controller is thus similar to two independent controllers, one for the heave mode and one for the pitch mode. This conclusion was partly anticipated in section 3 since the two eigenvalues of the plant response matrix **G** were noticed to be directly associated with the amplitude of the heave motion and pitching motion of the equipment. Finally, vibration amplification of the mass motion was observed at low frequencies because of phase shifts in the transducer conditioning electronics. This illustrates the difficulty of monitoring low-frequency velocity with an accelerometer and could cause instability for very high feedback gains. Significant active damping, equivalent to a viscous damping ratio of nearly 650%, could however be achieved with control gains below this stability limit. The use of a DC-coupled amplifier and appropriate high-pass filter could partly have removed this limitation. The excellent overall performance of the control is also partly due to the very flat frequency response of the transducers.

REFERENCES

1. S. A. COLLINS and A. H. VON FLOTOW 1991 *Presented at the* 42*nd Congress of the International Astronautical Federation, Montreal, Canada. Paper No. IAF*-91-289. Active vibration isolation for spacecraft.
2. D. KARNOPP, M. J. CROSBY and R. A. HARWOOD 1974 *American Society of Mechanical Engineers Journal of Engineering in Industry* **96**, 619–626. Vibration control using semi-active force generators.

3. C. R. FULLER, S. J. ELLIOTT and P. A. NELSON 1996 *Active Control of Vibration*. London: Academic Press.
4. D. W. SCHUBERT 1991 *Proceedings of the Conference on Recent Advances in Active Control of Sound and Vibration, Blacksburg, Virginia*, 448–463. Characteristics of an active vibration isolation system using absolute velocity feedback and force actuation.
5. A. M. BEARD, A. H. VON FLOTOW and D. W. SCHUBERT 1994 *Proceedings of IUTAM Symposium on the Active Control of Vibration, University of Bath, UK*. A practical product implementation of an active/passive vibration isolation system.
6. M. J. BALAS 1979 *Journal of Guidance and Control* **2**, 252–253. Direct velocity feedback control of large space structures.
7. M. SERRAND 1998 *M.Sc. thesis, University of Southampton*. Active isolation of base vibration.
8. P. GARDONIO, S. J. ELLIOTT and R. J. PINNINGTON 1996 *Institute of Sound and Vibration Research Technical Memorandum No.* 801, *University of Southampton*. User manual for the isolating system with two active mounts constructed at ISVR for the ASPN project final experiment.
9. P. GARDONIO and S. J. ELLIOTT 1999 *Proceedings of the active* 99 *conference, the* 1999 *Internationl Symposium on Active Control of Sound and Vibration*. Volume 1, page 117–128. Active control of structural vibration transmission between two plates connected by a set of active mounts.
10. G. B. WARBURTON 1951 *Proceedings of the Institute of Mechanical Engineering* **168**, 371–384. The vibration of rectangular plates.
11. B. NAYROLES 1987 *Journal de mécanique théorique et appliquée* (special issue) **6** (suppl.), 23–38. Functional monotony and diagonal control in synchronous vibration absorption.
12. S. J. ELLIOTT and C. C. BOUCHER 1994 *IEEE Transactions on Speech and Audio Processing* **2**, 521–530. Interaction between multiple feedforward active control systems.
13. G. F. FRANKLIN, J. D. POWELL and A. EMAMI-NAEINI 1994 *Feedback Control of Dynamic Systems*. Reading MA: Addison-Wesley, third edition.
14. S. SKOGESTAD and I. POSTLETHWAITE 1996 *Multivariable Feedback Control*. Chichester: Wiley.
15. S. J. ELLIOTT, M. SERRAND and P. GARDONIO 1999 *Journal of American Society of Mechanical Engineering*. Feedback stability limits for active isolation systems with reactive and inertial actuators (submitted).
16. L. MEIROVITCH 1990 *Dynamics and Control of Structures*. New York: Wiley.

APPENDIX: RELATION BETWEEN COLLOCATED DECENTRALIZED CONTROL AND INDEPENDENT MODEL-SPACE CONTROL

A.1. GENERAL CASE

The dynamics of a structure characterized by N modes can be fully identified with M appropriately positioned sensors provided $M \geqslant N$ [16]. The time-dependent modal co-ordinates a_j, for $j = 1$ to N, associated with each mode can be expressed in terms of the sensor signals v_i, for $i = 1$ to M, using a modal identification matrix $\mathbf{A}$ of dimension $(N \times M)$.

$$\mathbf{a} = \mathbf{A} \cdot \mathbf{v}. \tag{A1}$$

Reciprocally, the sensor signal vector can be derived from the modal co-ordinate vector using a modal reconstruction matrix $\mathbf{R}$ of dimension $(M \times N)$ such that

$$\mathbf{v} = \mathbf{R} \cdot \mathbf{a}. \tag{A2}$$

Similarly, assuming N modal control forces acting on a structure due to $P(P \geqslant N)$ point force actuators distributed over the controlled structure, the physical control forces f_{pk}, $k = 1$ to P, can be expressed in terms of the modal control forces f_{ml}, $l = 1$ to N, by a matrix $\mathbf{B}$ of dimension $(P \times N)$ such that

$$\mathbf{f}_p = \mathbf{B} \cdot \mathbf{f}_m. \tag{A3}$$

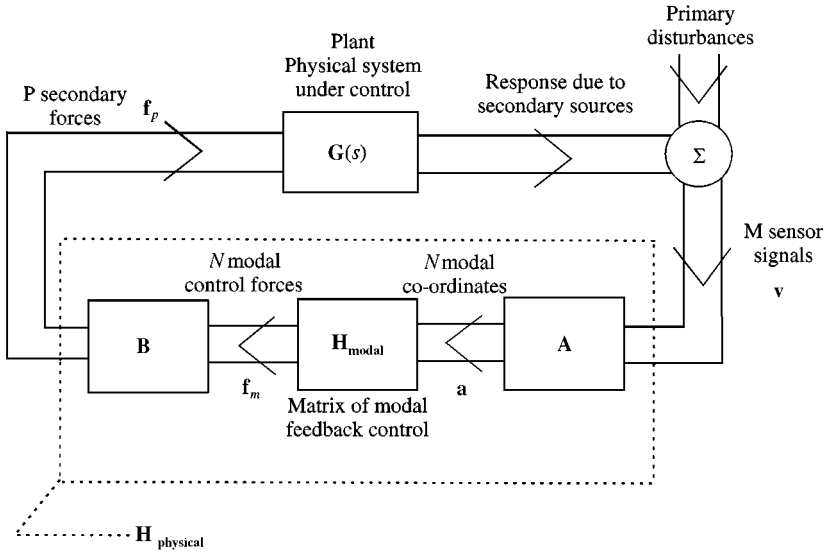

Figure A1. Physical equivalent electrical block diagram of a multichannel model feedback control system.

Reciprocally, the modal force vector $\mathbf{f}_m$ can be derived from the physical force vector $\mathbf{f}_p$ using a modal decomposition matrix $\mathbf{D}$ of dimension $(N \times P)$ such that

$$\mathbf{f}_m = \mathbf{D} \cdot f_p. \tag{A4}$$

The physical control relating the sensor signal vector $\mathbf{v}$ to the physical control force vector $\mathbf{f}_p$ can be expressed in a matrix form by $\mathbf{H}_{physical}$ such that

$$\mathbf{f}_p = \mathbf{H}_{physical} \cdot \mathbf{v}. \tag{A5}$$

Similarly assuming the implementation of a modal control, we can define a matrix $\mathbf{H}_{modal}$ relating the modal response component vector $\mathbf{a}$ to the modal control force vector $\mathbf{f}_m$:

$$\mathbf{f}_m = \mathbf{H}_{modal} \cdot \mathbf{a}. \tag{A6}$$

The physical control equivalent to the implementation of any modal control can then be derived using equations (A1), (A3) and (A6) as illustrated in Figure A.1:

$$\mathbf{H}_{physical} = \mathbf{B} \cdot \mathbf{H}_{modal} \cdot \mathbf{A}. \tag{A7}$$

Similarly, the modal control equivalent to the implementation of any physical control can be derived using equations (A2), (A4) and (A5):

$$\mathbf{H}_{modal} = \mathbf{D} \cdot \mathbf{H}_{physical} \cdot \mathbf{R}. \tag{A8}$$

For decentralized control, there are an equal number of sensors and actuators so that $M = P$. If it is also assumed that there are only as many modes as actuators and sensors then

$$N = M = P.$$

R and **D** are now squared matrix of rank N and therefore inversible provided the N sensors and actuators are properly located at N different positions on the structure. Therefore,

$$\mathbf{A} = \mathbf{R}^{-1} \quad \text{and} \quad \mathbf{B} = \mathbf{D}^{-1}. \tag{A9}$$

If each sensor is collocated with a corresponding actuator, it can be easily understood that the sensed modes and the forced modes are weighted with space-dependent coefficients such that

$$\mathbf{R} = \begin{bmatrix} \phi_1(x_1) & \phi_2(x_1) & \cdots & \phi_N(x_1) \\ \phi_1(x_2) & \phi_2(x_2) & & \vdots \\ \vdots & & \ddots & \\ \phi_1(x_N) & \cdots & & \phi_N(x_N) \end{bmatrix} = \mathbf{D}^{\mathrm{T}}, \tag{A10}$$

where $\phi_j(x_i)$ is the amplitude of the j^{th} mode at location i defined by x_i. For a decentralized physical control consisting of identical feedback gains g applied to each channel, the physical feedback control matrix is

$$\mathbf{H}_{physical} = -g \cdot \mathbf{I} \tag{A11}$$

therefore, using equations (A8) and (A10):

$$\mathbf{H}_{modal} = -\mathbf{D} \cdot g \cdot \mathbf{I} \cdot \mathbf{R} = -g \cdot \mathbf{D} \cdot \mathbf{D}^{\mathrm{T}}. \tag{A12}$$

If **D** is unitary to within a multiplicative factor c as in the two-channel case considered here and discussed in more detail below, then

$$\mathbf{D}^{\mathrm{T}} = c \cdot \mathbf{D}^{-1} \tag{A13}$$

and so

$$\mathbf{H}_{modal} = -g \cdot \mathbf{D} \cdot c \cdot \mathbf{D}^{-1} = -g \cdot c \cdot \mathbf{I} = c \cdot \mathbf{H}_{physical}. \tag{A14}$$

This means that a decentralized control system is equivalent to an independent modal-space control (IMSC) with modal feedback gains gc under the following four conditions:

- equal number of sensor/actuator pairs as modes characterizing the system behaviour,
- collocation of sensors and actuators,
- equal feedback gains g,
- sensors/actuators located on the structure such that **D** is unitary to within a multiplicative factor.

In order for the last condition, i.e., equation (A13), to be satisfied then one requires

$$\sum_{i=1}^{N} \phi_n^2(x_i) = c_n = c \quad \text{for all } n \tag{A15}$$

and

$$\sum_{i=1}^{N} \phi_n(x_i)\phi_m(x_i) = 0 \quad \text{for all } n \neq m. \tag{A16}$$

Equation (A15) is just a normalization condition and equation (A16) is a statement of the orthogonality of the modes, when evaluated at the transducer positions x_i. Decentralized control can also be equivalent to IMSC without satisfying equation (A15). The c_n values are then different from each other and an equal gain g in each independent control loop is equivalent to a modal control with different gains for each mode (in this case $\mathbf{D}\cdot\mathbf{D}^{\mathrm{T}}$ is diagonal but not equal to $\mathbf{I}$).

A.2. THE SPECIAL CASE OF THE TWO-CHANNEL CONTROLLER

For the special case of two-channel control described in this paper, the system to be isolated is a simple rigid body characterized by two axial degrees of freedom and therefore by two rigid-body modes in the frequency range of analysis: the heave mode and the pitch mode. From the symmetry of the isolation system, the heave and the pitching motions are entirely decoupled. The velocity $\dot{w}_h$ associated with the heave motion, which is the motion of the equipment centre of gravity, can then be expressed as

$$\dot{w}_h = \frac{(\dot{w}_1 + \dot{w}_2)}{2}, \tag{A17}$$

whereas the amplitude of the velocity $\dot{w}_p$ resulting from the pitching oscillations at the sensor locations is

$$\dot{w}_p = \frac{(\dot{w}_1 - \dot{w}_2)}{2}, \tag{A18}$$

where $\dot{w}_1$ and $\dot{w}_2$ are the velocities monitored by ideal control sensors on the mounted equipment at the vertical of the two active mounts, points 1 and 2 respectively (Figure 9).

The dynamics of the equipment can then be expressed in terms of modal quantities from the measured velocities using the matrix $\mathbf{A}$,

$$\begin{Bmatrix} \dot{w}_h \\ \dot{w}_p \end{Bmatrix} = \begin{bmatrix} \frac{1}{2} & \frac{1}{2} \\ \frac{1}{2} & -\frac{1}{2} \end{bmatrix} \cdot \begin{Bmatrix} \dot{w}_1 \\ \dot{w}_2 \end{Bmatrix} = \mathbf{A} \begin{Bmatrix} \dot{w}_1 \\ \dot{w}_2 \end{Bmatrix} \tag{A19}$$

so that

$$\begin{Bmatrix} \dot{w}_1 \\ \dot{w}_2 \end{Bmatrix} = \begin{bmatrix} 1 & 1 \\ 1 & -1 \end{bmatrix} \cdot \begin{Bmatrix} \dot{w}_h \\ \dot{w}_p \end{Bmatrix} = \mathbf{R} \begin{Bmatrix} \dot{w}_h \\ \dot{w}_p \end{Bmatrix}, \tag{A20}$$

where $\mathbf{A} = \mathbf{R}^{-1}$ and $\mathbf{A}$ and $\mathbf{R}$ are defined in equations (A1) and (A2).

Also, the heave and pitching control voltage signals u_h and u_p generated by a modal controller can be expressed in terms of the control voltages u_1 and u_2 input to the control shakers (Figure A.2). Assuming the two shakers have the same sensitivity,

$$\begin{Bmatrix} u_h \\ u_p \end{Bmatrix} = \begin{bmatrix} 1 & 1 \\ 1 & -1 \end{bmatrix} \cdot \begin{Bmatrix} u_1 \\ u_2 \end{Bmatrix} = \mathbf{D} \begin{Bmatrix} u_1 \\ u_2 \end{Bmatrix}, \tag{A21}$$

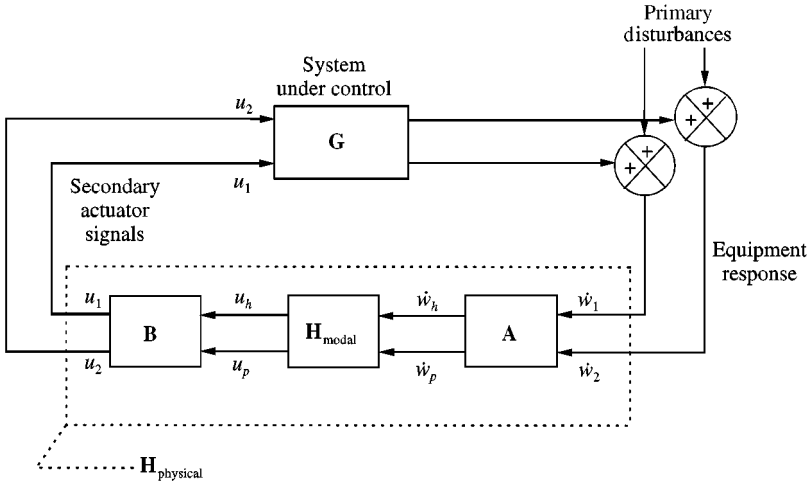

Figure A2. Physical equivalent electrical block diagram of a modal feedback control of two-degree-of-freedom system.

so that

$$\begin{Bmatrix} u_1 \\ u_2 \end{Bmatrix} = \begin{bmatrix} \frac{1}{2} & \frac{1}{2} \\ \frac{1}{2} & -\frac{1}{2} \end{bmatrix} \begin{Bmatrix} u_h \\ u_p \end{Bmatrix} = \mathbf{B} \begin{Bmatrix} u_h \\ u_p \end{Bmatrix}, \tag{A22}$$

where $\mathbf{B} = \mathbf{D}^{-1}$; $\mathbf{B}$ and $\mathbf{D}$ are defined in equations (A3) and (A4).

Because the actuators and sensors are collocated, $\mathbf{R} = \mathbf{D}^{\mathrm{T}}$. Also in this case, it can be noticed that

$$\mathbf{D}^{\mathrm{T}} = 2\mathbf{B} = 2\mathbf{D}^{-1} \tag{A23}$$

and so equation (A13) is satisfied. The independent control implemented experimentally is therefore equivalent to a modal control.